https://doi.org/10.46861/bmp.30.028 PŮVODNÍ PRÁCE/ORIGINAL PAPER

REE content of volcanic rocks and their weathered horizons in the Muria Volcanic Complex, Central Java, Indonesia

Sutarto Sutarto[1)]*, Adi Sulaksono[1)], Dema T. Laksana[1)], Anggita Mahyudani[1)], Ajimas P. Setiahadiwibowo[2)] and Muhammad Nurcholis[3)]

[1)]*Department of Geology, UPN Veteran Yogyakarta, Jl. Padjajaran, Yogyakarta 55283, Indonesia;*
e-mail: sutarto_geomin@upnyk.ac.id
[2)]*Department of Geophysical Engineering, UPN Veteran Yogyakarta, Jl. Padjajaran, Yogyakarta 55283, Indonesia*
[3)]*Department of Soil Science, UPN Veteran Yogyakarta, Jl. Padjajaran, Yogyakarta 55283, Indonesia*

Sutarto S, Sulaksono A, Laksana DT, Mahyudani A, Setiahadiwibowo AP, Nurcholis M (2022) REE content of volcanic rocks and their weathered horizons in the Muria Volcanic Complex, Central Java, Indonesia. Bull Mineral Petrolog 30(1): 28-37 ISSN: 2570-7337

Abstract

We investigated bedrock samples and their weathered horizons collected from the Muria Volcanic Complex (MVC), Central Java, Indonesia. In addition to petrographic study, samples were analysed using X-ray diffraction (XRD), inductively coupled plasma-atomic emission spectroscopy (ICP-AES), and inductively coupled plasma-mass spectrometry (ICP-MS) for mineral composition, major elements, and trace elements, respectively. Bedrock samples (n = 10) from the MVC have ΣREE ranging from 364 to 739 ppm (avg. 579 ppm). Basanite (n = 2) and phonotephrite (n = 2) are consistently high in ΣREE (659 - 739 ppm) compared with basaltic trachyandesite, trachyandesite, and trachyte. Apatite is the only REE-bearing mineral observed in basanite and phonotephrite (up to ~1 vol.%). The ΣREE is positively corelated with P_2O_5, which inversely corelates with SiO_2. The weathered horizons contain clay minerals that consist primarily of kaolinite ± halloysite. The REE content of the weathered horizons (n = 7) is up to 183 ppm higher than those of the bedrocks. The decrease in CaO and P_2O_5 indicates a fractionation of apatite at early stage of magma evolution, resulting in the depletion in the ΣREE content in the residual melt. We suggest that apatite is the major host of REE in the MVC alkali-rich, silica-undersaturated volcanic rocks, as evidenced by our petrographic and geochemical data. We also suggest that the increase in ΣREE in the weathered horizon is due to the presence of clay minerals, particularly kaolinite and halloysite.

Keywords: *apatite, REE, volcanic rocks, weathered horizons, clay minerals*

Received 20. 1. 2022; accepted 10. 3. 2022

Introduction

Rare earth elements (REEs) are of paramount importance in a modern society and are among the most critical of all raw materials (Wang et al. 2020). However, major supply of REEs is currently restricted to China, Brazil, Australia, United States, Canada, and India (Li et al. 2017; Zhang et al. 2020).

A number of weathering crust ion-adsorption type REE deposits has been discovered in South China. They are the main source of global HREEs and provide nearly the total global HREEs demand (Hoshino et al. 2016; Xie et al. 2016; Li et al. 2017; Goodenough et al. 2018). Ion -adsorption type REE deposits have also been discovered in Madagascar (Berger et al. 2014), Malawi (Le Couteur 2011), Brazil (Rocha et al. 2013), and Southeast Asia (Sanematsu et al. 2009). Most ion-adsorption type REE deposits are hosted in the weathered granite and felsic volcanic rocks (Bao, Zhao 2008; Sanematsu, Watanabe 2016; Qin et al. 2019), in which REEs are primarily hosted in less weather-resistant minerals (Chi et al. 2012; Li et al. 2017).

Exploration targets of REE in Indonesia include primary REE deposits associated with alkaline-peralkaline granitoids, secondary lateritic deposits, and monazite-xenotime by-products of placer-type tin mining. Granitoids and their weathered crusts are currently the main source of REEs in Indonesia (Setiawan et al. 2017). This paper presents the REE content in various alkali-rich, silica-undersaturated volcanic rocks in the Muria Volcanic Complex (MVC), Central Java, Indonesia, and their weathered horizons. Four weathering profiles of such volcanic rocks were carefully sampled, followed by detailed petrographic and geochemical studies.

Geological framework

The present day subduction of the Indian oceanic crust beneath the Sunda-Banda arc is well-documented in Hamilton (1977). This arc extends from the northern tip of the island of Sumatra to the southeast, continues eastward to the islands of Java, Bali, Lombok, Sumbawa, Sumba, and Flores. In Central and East Java, the axis of the volcanic arc corresponds to a set of active volcanoes, mainly calc-alkaline in nature with some low-K (tholeiitic) varieties (Hutchison 1981, 1982). They correspond to an approximately 200 km deep Benioff plane.

The MVC is situated behind the Pleistocene-Recent Sunda-Banda arc (Fig. 1). It is a complex of Pleistocene volcanoes that form a large peninsula in the northern part of Central Java. Most of the back arc volcanic centres in Central Java that include the MVC lie close to a major

distensional submarine geodynamic structure of which the trend is oblique to the arc (Letterier et al. 1990; the axis is indicated by dotted line on Figure 1). K-rich lavas have been erupted from the extinct MVC (van Bemmelen 1949); this composition is not consistent with the calk-alkaline affinity of the Pleistocene-Recent Sunda-Banda volcanic arc. The lower $^{87}Sr/^{86}Sr$ ratios of leucite-bearing lavas of the MVC also suggest that they are genetically related to rifting and represent a back-arc volcanism (Cundari 1980). The MVC K-rich volcanic rocks were generated by melting of mantle sources enriched in incompatible elements during previous subduction events, and possibly involving a contribution of subcontinental mantle (Letterier et al. 1990).

Local geology

The MVC volcanic activities can be divided into two main products i.e., Mount Genuk (2.00 - 0.49 Ma) in the north and Mount Muria (0.84 - 0.32 Ma) in the south (McBirney et al. 2003; Fig. 2). These volcanoes lie on the Middle Miocene calcareous sedimentary sequence of the Bulu Formation. Our geological mapping shows that Mount Genuk is composed of basaltic trachyandesite in the center (main volcanic vent) surrounded by volcaniclastic deposits of the Ujungwatu Formation and pyroclastic deposits. Trachyte and basaltic trachyandesite are also observed in the distal facies (possibly secondary vent; Fig. 2). Mount Muria is composed of more varied volcanic rocks i.e., basanite, phonotephrite, trachyandesite and basaltic trachyandesite (Fig. 2). These volcanic rocks are surrounded by widespread pyroclastic deposits in the distal facies.

Sampling and analytical methods

A total of 16 samples from bedrocks and their weathered horizons were collected from the MVC. The most complete weathering profile in the MVC consists of trachyandesite bedrock (TA-Bed), horizon C (a layer of partially altered bedrock; TA-Wth-C), horizon B (where soluble minerals and clays accumulate; TA-Wth-B) and horizon A (near-surface horizon containing humified organic matter; TA-Wth-A). A basanite outcrop (B-1-Bed) is associated only with horizon C (B-1-Wth), whereas trachyte bedrocks T-1-Bed and T-2-Bed have only horizon C (T-1-Wth) and horizon A (T-2-Wth), respectively. Six unweathered samples such as basanite (B-1), phonotephrite (PT-1, PT-2) and basanite trachyandesite (BTA-1, BTA-2, BTA-3) were also collected.

All samples were air-dried at 20 - 30 ºC for four weeks, then were quartered and powdered using mortar and pestle. Four polished thin sections of bedrocks were prepared. The abundances of rock-forming minerals in the bedrock were determined under optical microscope. The bulk mineralogy of the samples was analysed using XRD at UPN Veteran Yogyakarta. Mineral identification was accomplished using the COD reference database of MATCH! software. The bulk rock geochemical analyses for both major and trace elements were carried out at ALS Geochemistry, Brisbane, Australia. Major elements have been analysed by ICP-AES (preceded by peroxide fusion), whereas trace elements were measured using ICP -MS (preceded by lithium borate fusion).

Results

Petrography of volcanic rocks

A total of 10 volcanic rock samples in this study include basanite (n = 2), phonotephrite (n = 2), basaltic trachyandesite (n = 3), trachyandesite (n = 1), and trachyte (n = 2). Two basanite samples (B-1-Bed and B-2; Fig. 3A, B) contain olivine, pyroxene, plagioclase, and feldspathoid phenocrysts up to 30 vol.%, generally from 0.5 to 4 mm in size, in a groundmass that consists of mainly plagioclase, feldspathoid, apatite, and opaque minerals (magne-

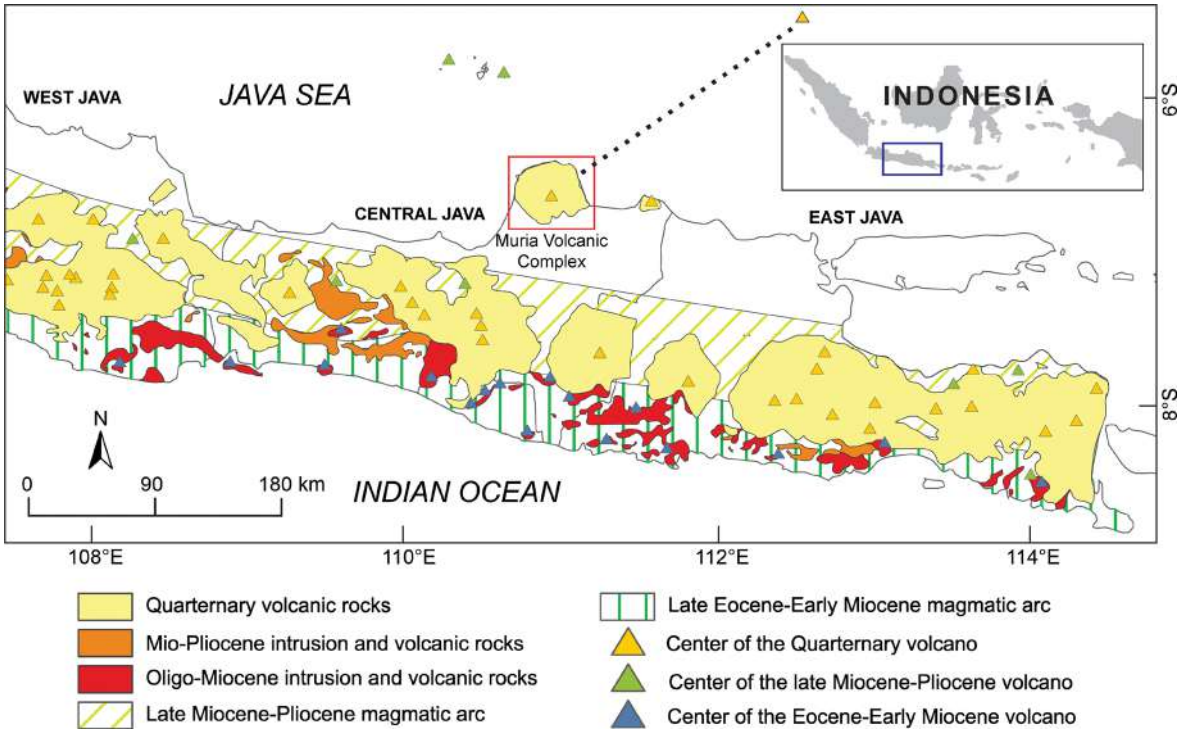

Fig. 1 *The distribution of magmatic-volcanic arcs in Java island, Indonesia. The MVC (red square) is situated behind the Pleistocene-Recent Sunda-Banda arc, forming a large peninsula in the northern part of the island.*

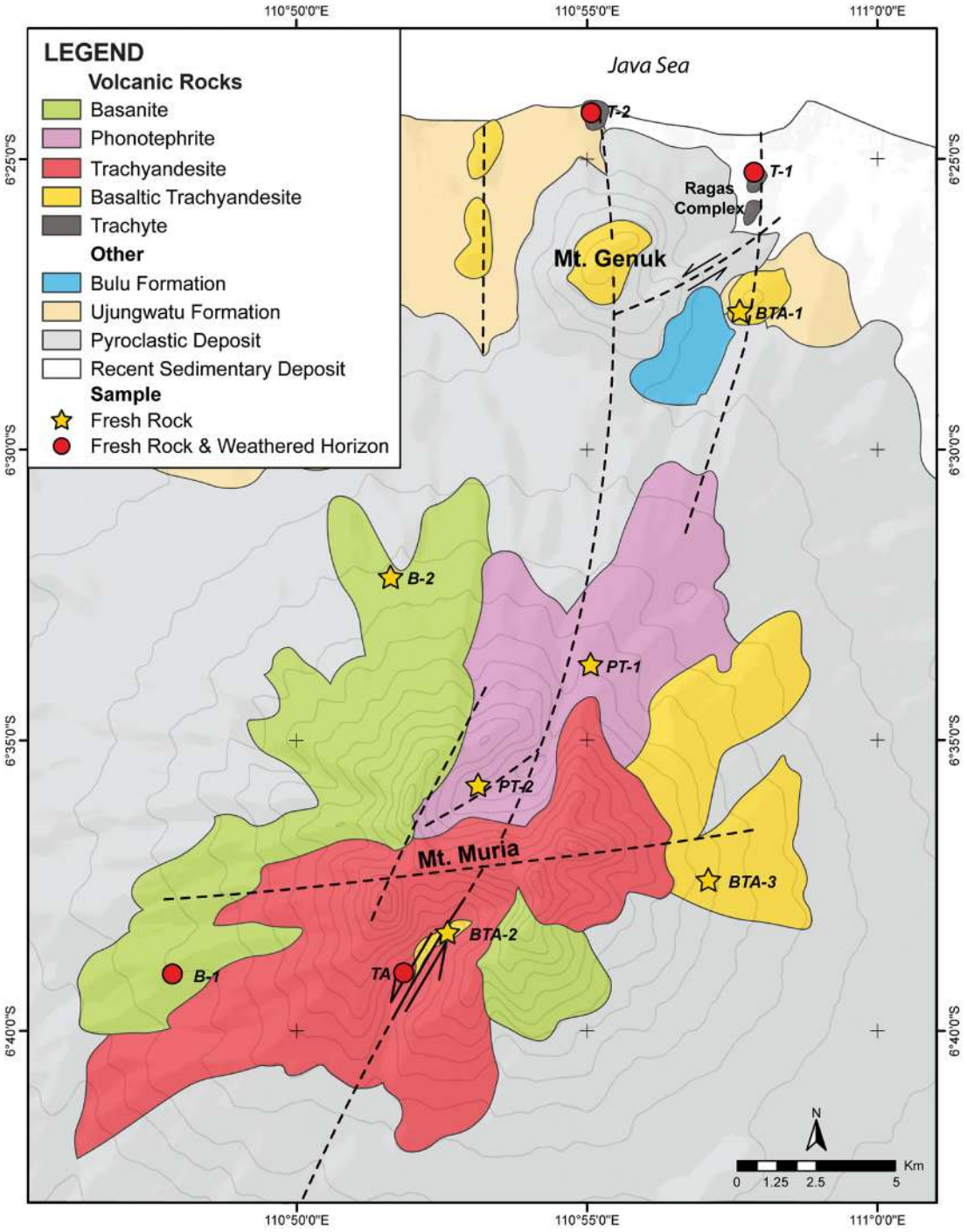

Fig. 2 *Geological map of the Muria Volcanic Complex (MVC).*

Fig. 3 *Representative photomicrographs of the MVC volcanic rock samples. A. Basanite (sample B-1-Bed) with olivine and feldspathoid phenocrysts, set in the groundmass composed of plagioclase, feldspathoid, apatite, and opaque minerals. B. Basanite (sample B-2), showing phenocrysts of olivine, pyroxene, and feldspathoid. Also shown is the pyroxene corona on olivine. C. Apatite inclusions in pyroxene (basanite; sample B-1-Bed). D. Apatite inclusion in feldspathoid (basanite; sample B-2). E. Phonotephrite of sample PT-1, showing phenocryst crystals of pyroxene. The phenocrysts are set in the fine-grained plagioclase, feldspathoid, opaque minerals (magnetite and ilmenite), apatite, and glass groundmass. F. Phonotephrite of sample PT-2, showing phenocrysts of amphibole, pyroxene, and plagioclase. These phenocrysts are set in the fine-grained plagioclase, feldspathoid, opaque minerals (magnetite and ilmenite), apatite, and glass groundmass. G. Trachyandesite of sample TA-Bed, showing a porphyritic texture with pyroxene phenocrysts. The phenocrysts are set in a crystal groundmass that contains mainly plagioclase, K-feldspar, and opaque minerals (magnetite and ilmenite). H. Trachyte (sample T-2-Bed), which shows a typical trachytic texture, where acicular to tabular feldspar of groundmass shows flow structure. Abbreviations: Ap, apatite; Amp, amphibole; Foid, feldspathoid; Kfs, K-feldspar; Mag, magnetite; Ol, olivine; Pl, plagioclase; Px, pyroxene; PPL, Plane-polarized light; XPL, Crossed polars.* →

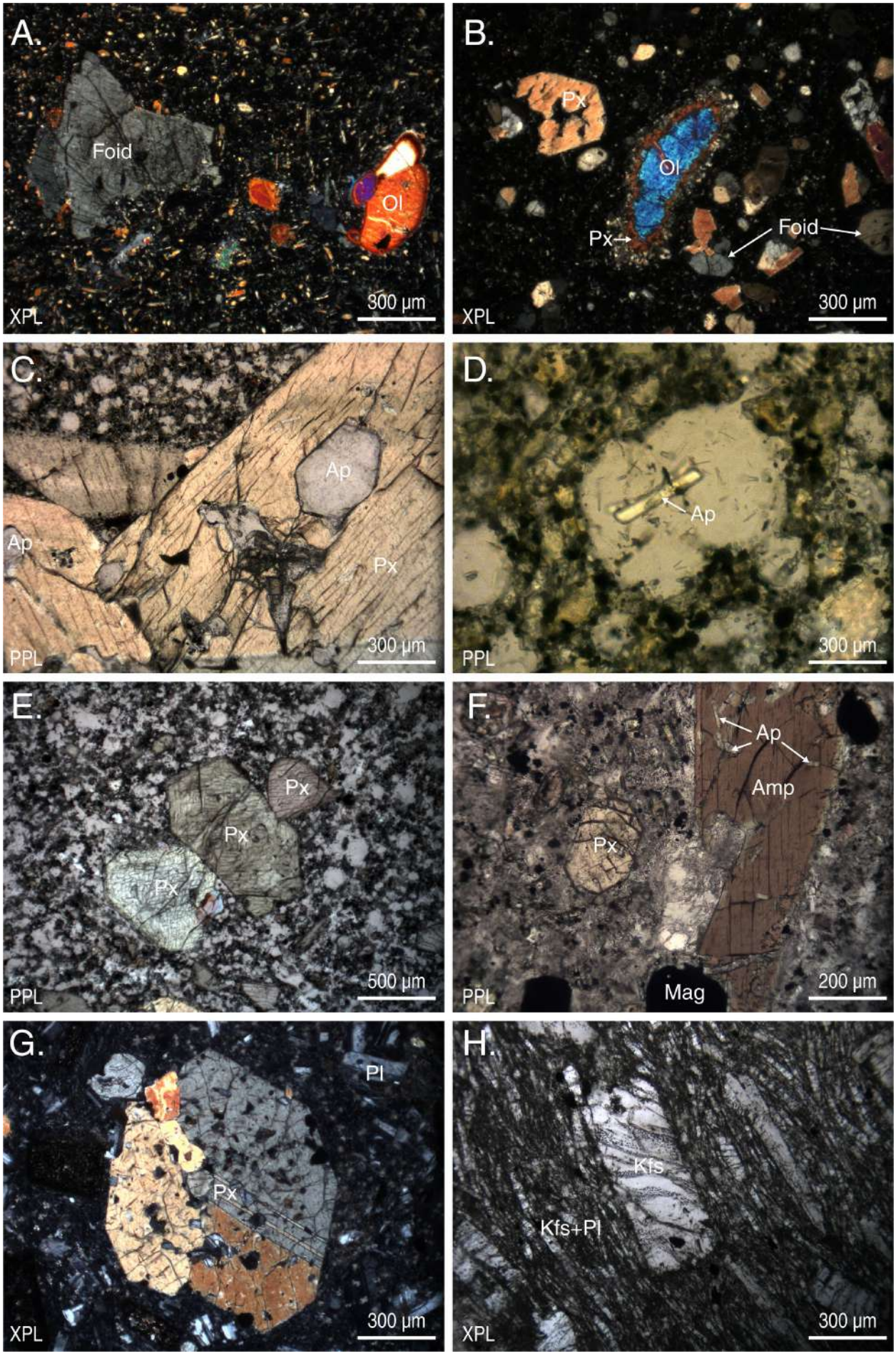
A.
Foid
Ol
XPL
300 µm
B.
Px
Ol
Px
Foid
XPL
300 µm
C.
Ap
Ap
Px
PPL
300 µm
D.
Ap
PPL
300 µm
E.
Px
Px
Px
PPL
500 µm
F.
Ap
Amp
Px
Mag
PPL
200 µm
G.
Pl
Px
XPL
300 µm
H.
Kfs
Kfs+Pl
XPL
300 µm

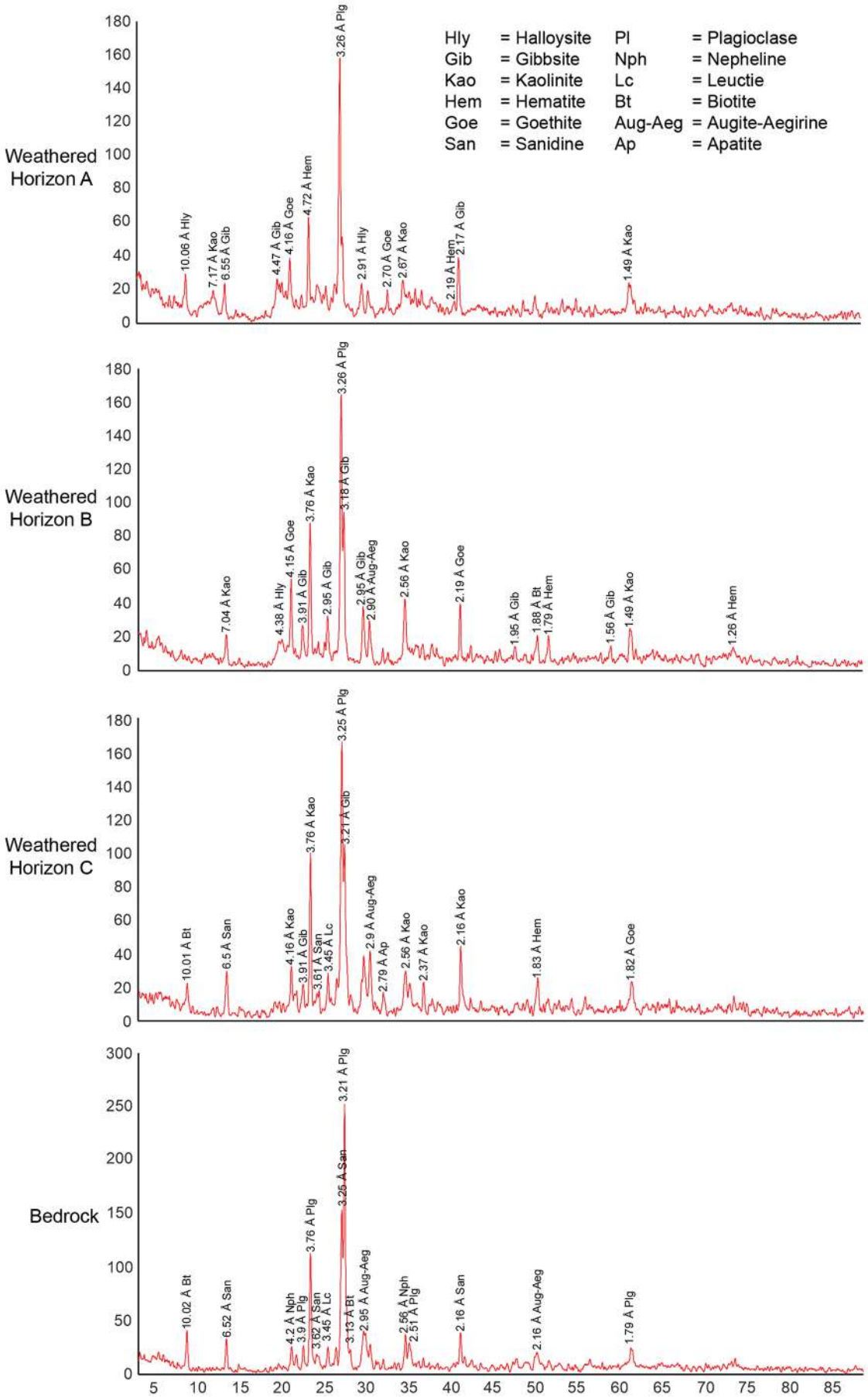

Fig. 4 *XRD patterns of trachyandesite bedrock and its weathered horizons A, B, and C. The dominant minerals in the bedrock are plagioclase, sanidine, and augite, whereas kaolinite and Fe-oxides are observed mostly in the weathered horizon A, B, and C. Halloysite is observed in the weathered horizon A and C.*

tite and ilmenite). The olivine, pyroxene, plagioclase, and feldspathoid phenocrysts are euhedral to anhedral, and commonly host apatite inclusions (Fig. 3C, D). Pyroxene corona on olivine is common (Fig. 3B). Sample B-1-Bed shows that groundmass crystals have fluidal texture.

Phonotephrite of sample PT-1 is characterized by a strong porphyritic texture (Fig. 3E). Phenocryst crystals (~30 vol.%) are up to 2 mm long and consist of olivine, pyroxene, amphibole, plagioclase, and feldspathoid. The phenocrysts are set in the fine-grained matrix composed of plagioclase, feldspathoid, opaque minerals (magnetite and ilmenite), apatite, and less commonly glass. Sample PT-2 is characterized by a weak porphyritic texture (Fig. 3F). Phenocrysts are up to 4 mm long and comprise up to ~20 vol.% of rock. Phenocryst crystals consist mainly of amphibole and less commonly pyroxene, biotite, plagioclase and feldspathoid. These phenocrysts are set in the fine-grained groundmass formed by plagioclase, feldspathoid, opaque minerals (magnetite and ilmenite), apatite, and less commonly glass. Apatite inclusions in phenocryst crystals are common in both samples PT-1 and PT-2 (Fig. 3F).

Basaltic trachyandesites (BTA-1, BTA-2, BTA-3) are characterized by a weak porphyritic texture. Phenocryst crystals are up to 2.5 mm long and consist of pyroxene, amphibole, biotite, plagioclase, and less commonly K-feldspar. These phenocrysts are set in the fine-grained matrix composed of plagioclase, K-feldspar, magnetite, il-

Table 1 *Whole-rock major and trace element concentrations for the MVC samples. Abbreviations (sample codes): B, basanite; T, trachyte; TA, trachyandesite; PT, phonotephrite; BTA, basaltic trachyandesite; Bed, bedrock; Wth, weathered horizon*

Sample	B-1-Bed	B-1-Wth	B-2	T-1-Bed	T-1-Wth	T-2-Bed	T-2-Wth	TA-Bed	TA-Wth-C	TA-Wth-B	TA-Wth-A	PT-1	PT-2	BTA-1	BTA-2	BTA-3
SiO_2 (wt.%)	44.70	32.10	45.30	60.90	58.60	65.10	52.10	53.60	54.20	53.60	45.10	48.30	50.50	50.90	52.00	50.30
Al_2O_3	14.65	27.20	16.35	20.80	21.00	20.20	24.60	17.60	18.25	20.70	24.00	15.65	18.75	17.65	19.05	17.65
Fe_2O_3	10.15	15.50	11.15	3.42	4.05	1.87	3.61	8.88	6.96	6.39	12.25	9.74	7.66	7.64	8.30	8.24
CaO	12.35	0.35	12.70	1.48	1.06	0.61	0.65	5.83	6.17	2.22	0.80	10.80	7.20	6.75	7.14	7.85
MgO	6.32	0.51	5.98	0.24	0.31	0.04	0.36	2.33	2.60	1.03	1.00	5.29	3.05	2.48	2.24	3.08
Na_2O	2.97	0.15	1.83	3.97	3.52	5.80	2.79	3.24	2.89	2.40	1.44	3.13	3.40	3.05	3.76	3.27
K_2O	4.72	0.34	3.91	7.24	6.83	6.74	4.07	4.95	4.83	5.40	3.40	5.55	5.66	2.42	2.78	4.56
TiO_2	1.08	1.67	1.21	0.25	0.33	0.18	0.38	0.85	0.90	1.02	1.22	1.05	0.86	0.73	0.79	0.78
MnO	0.20	0.42	0.22	0.13	0.18	0.15	0.26	0.13	0.15	0.08	0.20	0.19	0.19	0.17	0.17	0.20
P_2O_5	0.98	0.74	1.06	0.07	0.05	0.01	0.07	0.61	0.57	0.65	0.45	1.05	0.53	0.60	0.67	0.65
SrO	0.19	0.09	0.19	0.16	0.12	0.02	0.02	0.11	0.09	0.07	0.05	0.18	0.22	0.17	0.18	0.22
BaO	0.17	0.36	0.12	0.24	0.25	0.03	0.03	0.13	0.12	0.13	0.14	0.27	0.14	0.17	0.17	0.13
Total	98.48	79.43	100.02	98.90	96.30	100.75	88.94	98.26	97.73	93.69	90.05	101.20	98.16	92.73	97.25	96.93
La (ppm)	176	213	159	134	138	90	135	106	111	124	150	188	167	106	117	171
Ce	314	418	288	261	287	159	273	185	198	188	262	286	289	185	207	294
Pr	33.4	38.6	32.2	20.3	20.8	14.9	20.7	20.5	21.6	23.7	28.7	27.5	30.3	20.5	21.9	31.0
Nd	121	138	119	62.8	65.6	43.3	65.7	75.3	77.5	85.5	103	90.9	110	75.9	78.5	108
Sm	20.70	23.50	21.20	9.05	9.72	6.36	9.51	13.00	13.60	14.65	18.10	14.20	18.35	13.10	13.55	18.30
Eu	5.75	6.48	5.89	2.91	2.95	1.58	2.10	3.55	3.53	3.79	4.74	3.79	5.17	3.52	3.64	4.81
Gd	15.60	17.65	16.85	6.15	6.79	4.94	7.25	10.05	10.55	11.30	13.75	10.15	13.75	9.64	9.93	13.50
Tb	1.83	2.10	1.98	0.84	0.85	0.74	1.02	1.29	1.33	1.41	1.66	1.21	1.66	1.23	1.29	1.62
Dy	8.15	9.28	9.02	4.35	4.48	4.42	5.80	6.34	6.60	6.81	8.31	5.78	7.82	6.18	6.52	7.78
Ho	1.32	1.48	1.45	0.83	0.84	0.98	1.24	1.13	1.18	1.21	1.51	0.98	1.34	1.13	1.18	1.32
Er	3.05	3.48	3.49	2.29	2.27	3.07	4.00	3.06	3.11	3.14	3.96	2.42	3.36	2.94	3.28	3.19
Tm	0.40	0.45	0.45	0.35	0.34	0.54	0.67	0.43	0.45	0.45	0.54	0.31	0.46	0.44	0.48	0.44
Yb	2.22	2.83	2.58	2.20	2.22	3.86	4.75	2.61	2.65	2.74	3.39	1.99	2.76	2.51	2.93	2.78
Lu	0.35	0.45	0.39	0.35	0.34	0.64	0.81	0.40	0.41	0.42	0.51	0.29	0.42	0.40	0.46	0.43
Y	35.9	37.8	40.3	22.6	23.8	29.8	39.0	30.6	32.7	32.9	41.1	26.1	36.3	29.5	33.9	36.9
ΣREE	739	913	701	530	566	364	570	458	484	500	641	659	687	457	501	695
Th	29.8	48.2	29.6	38.1	37.2	40.5	47.1	25.6	29.0	32.9	38.2	44.8	37.2	23.7	31.3	42.2
U	5.07	7.24	4.87	1.82	3.08	4.82	11.05	5.11	6.35	7.41	7.95	9.99	7.8	4.29	6.29	6.77
Zr	272	435	296	285	281	515	637	234	253	310	351	240	336	218	276	337
Hf	5.5	8.6	6.0	5.2	5.3	9.4	11.6	5.1	5.4	6.4	7.4	4.5	6.3	4.6	5.7	6.3
Sn	1	2	2	1	1	1	2	1	2	1	3	1	1	2	2	1
Nb	84.0	136	62.2	40.8	43.4	39.1	50.2	41.0	38.4	43.3	55.0	205	79.0	39.7	53.9	89.7
Ba	1,630	3,390	1,080	2,230	2,260	261	278	1,220	1,090	1,220	1,250	2,500	1,290	1,650	1,570	1,290
Cr	160	150	120	<10	10	<10	10	30	50	70	50	90	50	40	10	20
Cs	5.29	1.90	7.83	10.8	6.19	8.84	8.60	9.66	7.90	6.49	8.37	5.67	9.23	4.27	3.77	9.45
Ga	18.4	31.0	20.3	20.2	20.9	24.1	30.4	20.9	21.3	24.5	28.5	17.5	21.4	20.6	22.1	21.2
Rb	188	14.9	261	200	167	269	176	187	173	196	144	218	167	49.3	58.8	272
Sr	1,610	766	1,610	1,390	1,030	160	141	945	765	606	456	1,540	1,910	1,420	1,520	1,930
Ta	3.1	4.7	2.5	1.6	1.7	1.3	1.6	1.6	1.6	1.8	2.2	7.7	3.1	1.4	1.9	3.6
V	355	244	371	39	88	20	68	242	269	270	352	330	226	216	207	248
Rb/Sr	0.12	0.02	0.16	0.14	0.16	1.68	1.25	0.20	0.23	0.32	0.32	0.14	0.09	0.03	0.04	0.14

menite, apatite, and glass. The rutile-magnetite assemblage occurs as a reaction rim on biotite phenocrysts. Apatite is common inclusion mineral in silicate phenocrysts.

A trachyandesite sample (TA-Bed) is characterized by a porphyritic texture of pyroxene, amphibole, and biotite phenocrysts (up to 60 vol.%; Fig. 3G). These phenocrysts are 0.5 to 2 mm in length. The pyroxene phenocrysts particularly host zircon inclusions. The phenocrysts are set in a crystal groundmass that contains mainly plagioclase, K-feldspar, and opaque minerals (magnetite and ilmenite). Apatite crystals are observed as inclusion in the phenocryst crystals as well as in the groundmass.

Trachyte samples (T-1-Bed, T-2-Bed) contain plagioclase, K-feldspar, pyroxene, olivine, glass, and accessory magnetite (Fig. 3H). This rock shows a weak porphyritic texture with mainly plagioclase and K-feldspar phenocrysts (less commonly olivine and pyroxene), set in the fine-grained groundmass composed of plagioclase, K-feldspar and glass. Phenocrysts are generally 0.2 to 2 mm in size. Plagioclase and K-feldspar comprise up to 75 vol.% of rocks. These trachyte samples show a typical trachytic texture, where acicular to tabular feldspar groundmass shows fluidal texture.

Bulk rock mineralogy

Bedrocks and their weathered horizons A, B, and C from trachyandesite were analysed for their mineralogy by XRD (Fig. 4). K-feldspar and plagioclase are the dominant minerals in the trachyandesite bedrock. Clay minerals are observed in the weathered horizons A, B, and C. Kaolinite is preserved in all horizons, whereas halloysite occurs preferentially in horizon A.

Whole-rock geochemistry

Results of bulk rock geochemical analyses are presented in Table 1. The bedrock samples contain SiO_2 and K_2O ranging 44.70 - 65.10 wt.% and 2.42 - 7.24 wt.%, respectively. Silica content generally increases with decreasing TiO_2 content. Trachyte, trachyandesite, and basaltic trachyandesite samples are classified into shoshonite series in the SiO_2 vs. K_2O diagram, whereas basanite and phonotephrite fall into the leucitic series (Fig. 5). The Harker diagrams indicate that the TiO_2, Fe_2O_3, MnO, MgO, CaO, and P_2O_5 decrease with increasing of SiO_2 content, whereas K_2O, Na_2O, and Al_2O_3 are positively correlated with the SiO_2 content (Fig. 6). Weathered horizons were not plotted in the Harker diagrams.

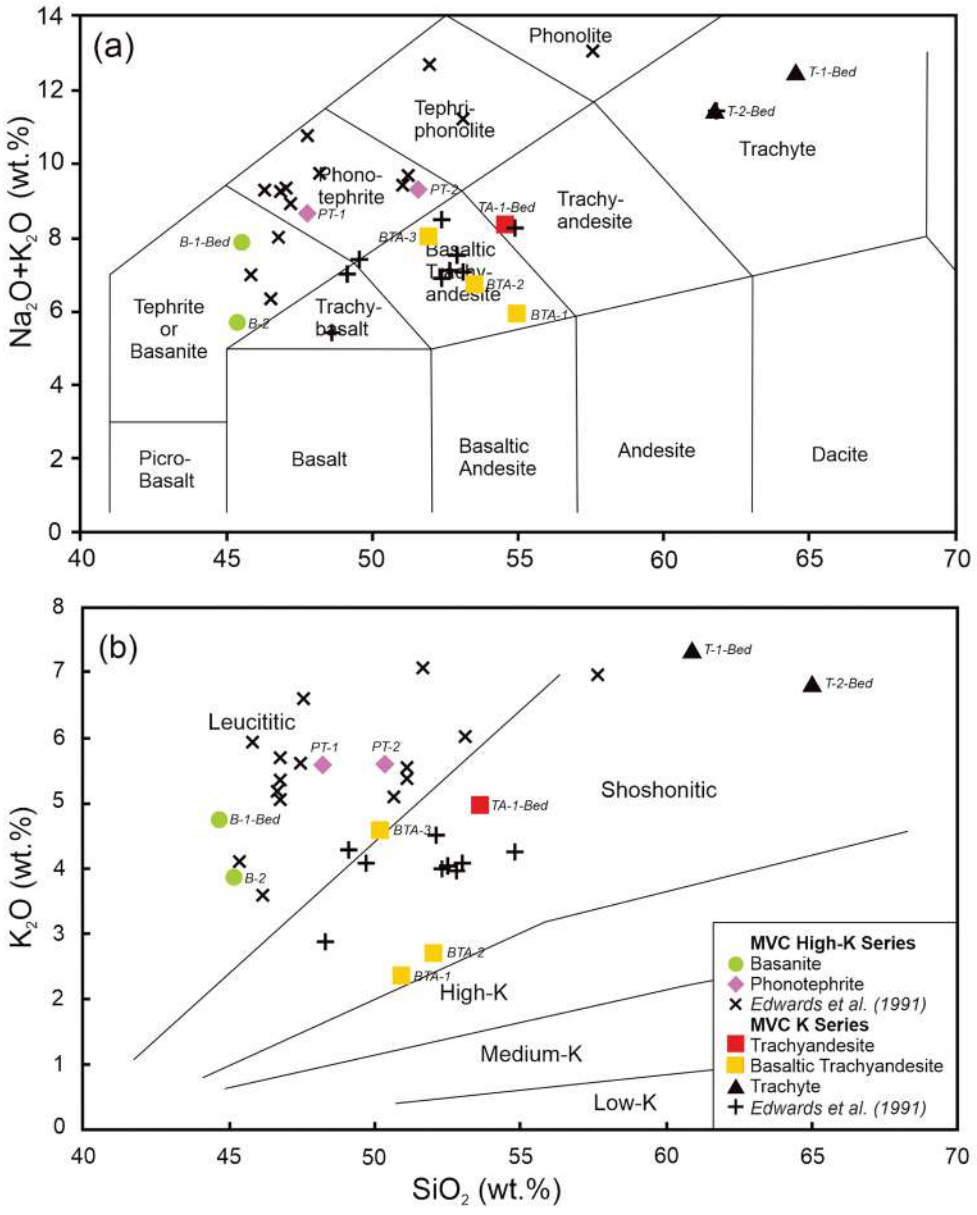

Fig. 5 *A. Total alkalis (Na_2O+K_2O) vs. silica (SiO_2) diagram of the volcanic rocks from the MVC. B. K_2O vs. SiO_2 diagram of the volcanic rocks from the MVC. Our data are fit with those from Edwards et al. (1991). Basanite and phonotephrite are classified into the MVC high-K series, whereas trachyandesite, basaltic trachyandesite and trachyte belong to the MVC K series (see Edwards et al. 1991).*

The whole-rock REE concentrations in both bedrock and weathered horizon were analysed. The P_2O_5 and CaO contents in the bedrocks are positively correlated with ΣREE (Fig. 7). Bedrock samples from the MVC have REE contents ranging from 364 to 739 ppm, whereas the weathered horizons are more enriched in REE (484 to 913 ppm). Basanite and phonotephrite samples have highest ΣREE ranging from 659 to 739 ppm. Chondrite-normalized REE patterns show that both bedrock and weathered horizon samples show a systematic minor HREE-enriched U-shaped patterns (Fig. 8). Small positive Eu anomaly is observed in trachyte, whereas the other three bedrock samples show negligible Eu anomalies.

Discussion

Fractional crystallization

The SiO_2 contents of samples studied are very low to intermediate, ranging from 44.70 to 65.10 wt.%. These samples have Rb/Sr ratios of 0.03 - 1.68. Such low to intermediate SiO_2 and low Rb/Sr ratios suggest that the magmas were weakly differentiated. Negative correlations between TiO_2, Fe_2O_3, MnO, MgO, CaO, P_2O_5, and SiO_2 content suggest that the magmas likely underwent fractional crystallization during magmatic differentiation. The decrease in Fe_2O_3, MgO, CaO, and P_2O_5 indicates removal of mafic minerals and apatite. The ΣREE content decreases with decrease of CaO and P_2O_5, indicating that the fractionation of apatite consumed REE from the crystallizing melt significantly. Thus apatite is likely the major host for REE in the fresh volcanic rock in the MVC. This is supported by the abundant presence of apatite in basanite and phonotephrite (Fig. 3).

Silica is positively correlated with some major oxides such as K_2O, Na_2O, and Al_2O_3, indicating that these elements were not fractionated in the early stage of magma evolution. They are mainly partitioned in minerals observed in the samples such as plagioclase and K-feldspar. The absence of an early plagioclase fractionation is evidenced by the lack of negative Eu anomalies in the chondrite-normalized diagram (Fig. 8).

Mineralogical and geochemical evolution of the laterite profiles

Bedrocks are the primary source of REEs in the weathering horizons. To form ion-adsorption type REE deposits, the parent rocks must have a sufficient amount of REEs, which are hosted in weatherable minerals e.g., fluorocarbonates, allanite, titanite (Chi et al. 2012) and possibly apatite. Apatite is absent in REE-enriched weathered horizons (Fig. 4, horizons A and B). Therefore, REEs were likely bound to the clay minerals during weathering

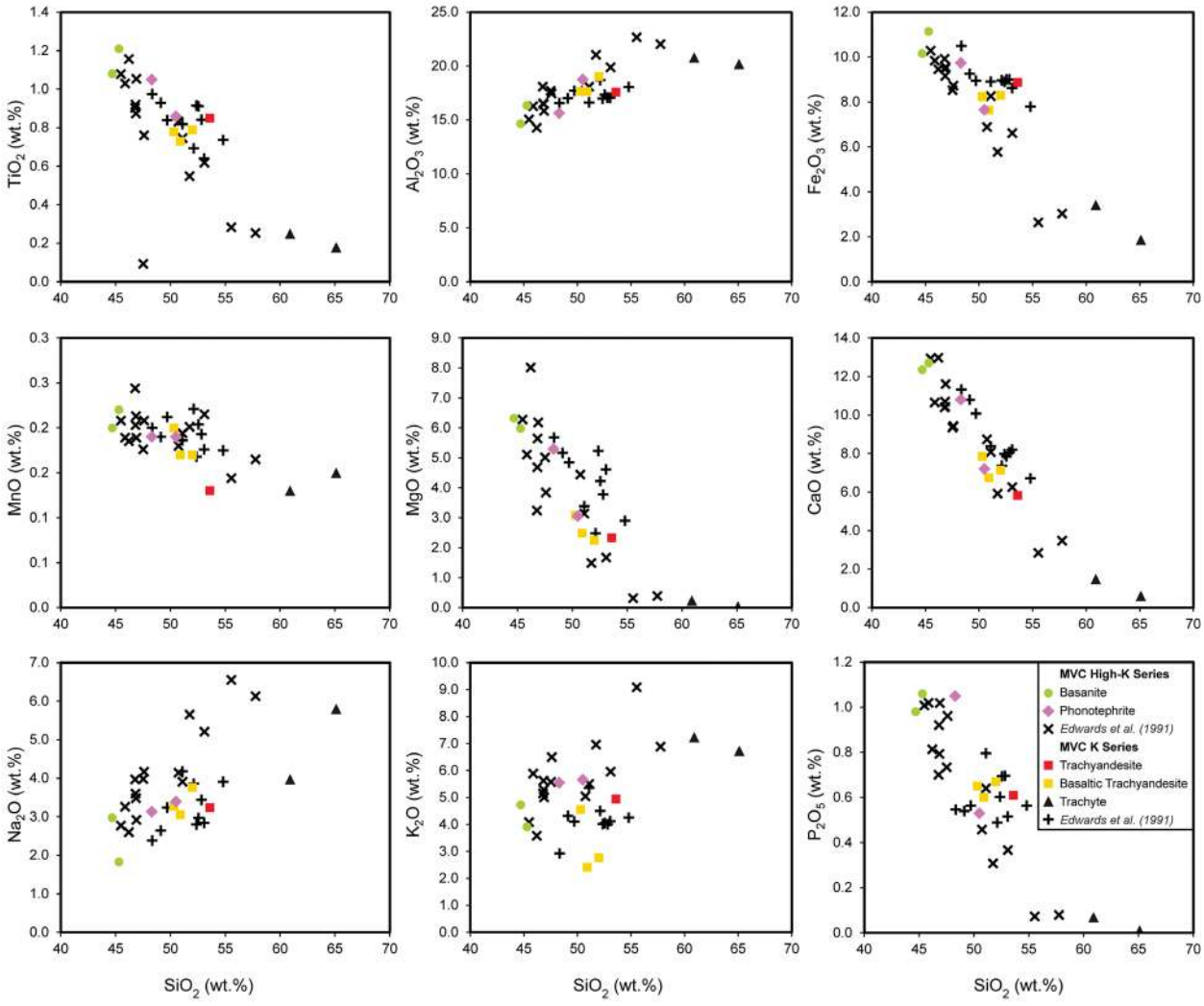

Fig. 6 *Harker diagrams of major elements oxides of the MVC rock samples. Our data are generally consistent with the data from Edwards et al. (1991).*

rather than to residual REE-bearing apatite. We suggest that apatite was decomposed during weathering, providing REEs to be deposited in weathered horizons.

Kaolinite and halloysite formed during the weathering of mainly plagioclase and K-feldspar in the samples studied. The results of XRD measurements on trachyandesite profile show that kaolinite is preserved in all horizons. Halloysite occurs preferentially in horizon A, in which ΣREE is significantly enriched. The sorption ability of halloysite for REEs is presumably not very different from that of kaolinite (Mukai et al. 2020). Thus we interpret that in addition to kaolinite (Wu et al. 1990; Bao et al. 2008), halloysite in the particles possibly plays a role in the enrichment of REEs in the weathered horizons.

Conclusions

The REE content of volcanic rocks samples collected from the MVC varies from 364 to 739 ppm. Alkali-rich, silica -undersaturated rocks such as basanite and phonotephrite samples have highest ΣREE ranging from 659 to 739 ppm. Apatite is likely the major host for REE in this type of rock as evidenced by our petrographic and chemical data. The decrease in CaO and P_2O_5 indicates preferential crystallization of apatite at early stage of magma evolution, resulting in the depletion in the ΣREE content of the MVC differentiated volcanic rock. The ΣREE increases in the weathered horizon, thus we suggest that in the MVC the increase in ΣREE in the weathered horizon is due to the presence of clay minerals, particularly kaolinite and halloysite.

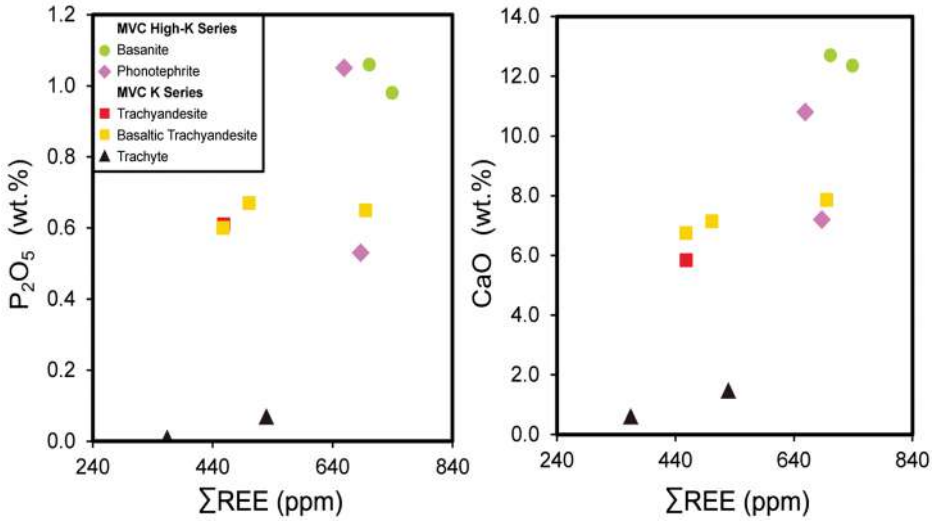

Fig. 7 *A. The P_2O_5 vs. ΣREE diagram. B. The CaO vs. ΣREE diagram. Both P_2O_5 and CaO contents in the bedrocks are positively correlated with ΣREE.*

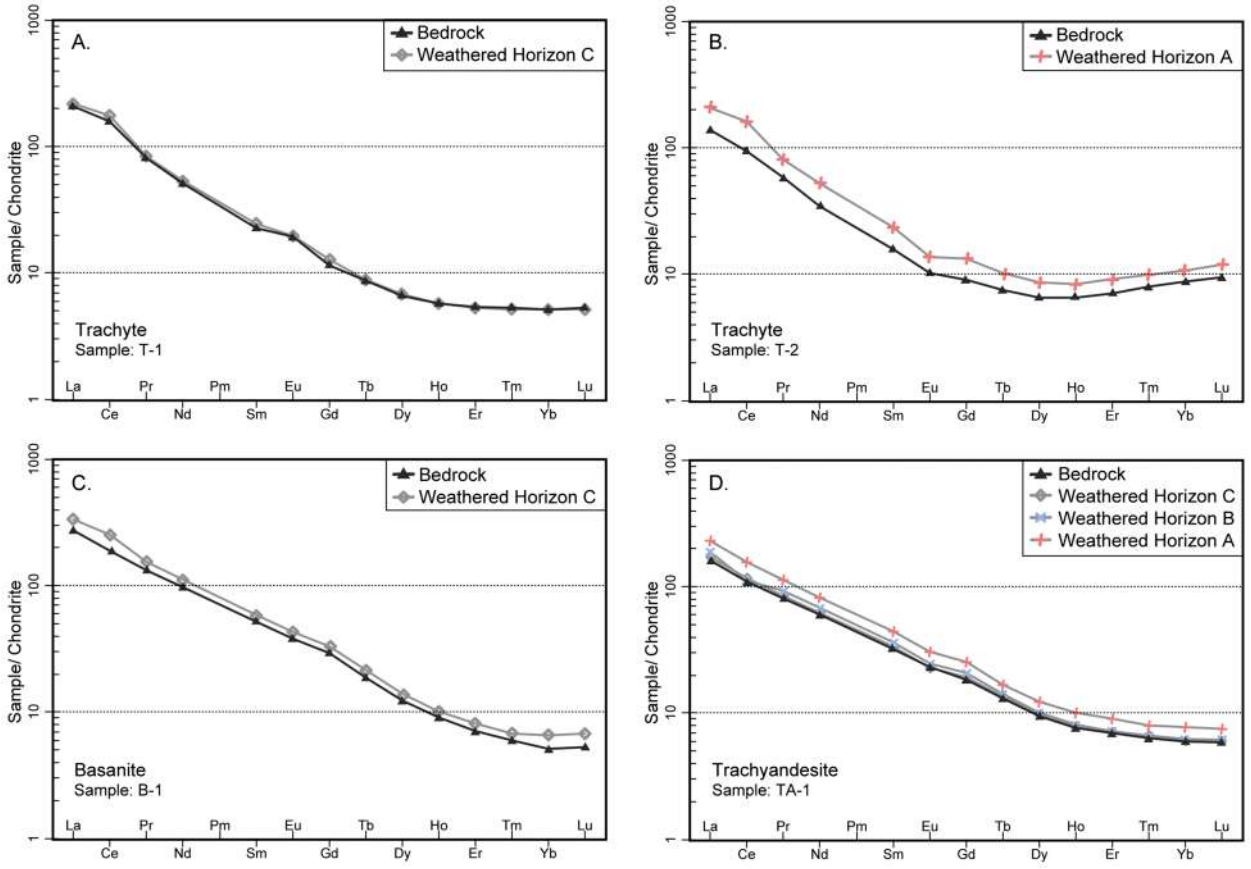

Fig. 8 *Chondrite-normalized REE patterns for both bedrocks and weathered horizons.*

Acknowledgement

This project was funded by the Ministry of Education, Culture, Research, and Technology, Indonesia. We acknowledge Mr. Agus for his support during the fieldwork.

References

Bao ZW, Zhao ZH (2008) Geochemistry of mineralization with exchangeable REY in the weathering crusts of granitic rocks in South China. Ore Geol Rev 33: 519-535

Bemmelen RW VAN (1949) The Geology of Indonesia. Martinus Nijhoff, Den Haag

Berger A, Janots E, Gnos E, Frei R, Bernier F (2014) Rare earth element mineralogy and geochemistry in a laterite profile from Madagascar. Appl Geochem 41: 218-228

Chi RA, Tian J, Luo XP, Xu ZG, He ZY (2012) The basic research on the weathered crust elution-deposited rare earth ores. Nonferrous Metal Sci Engineer 3: 1-13 (in Chinese with English abstract)

Cundari A (1980) Role of subduction in the genesis of leucite-bearing rocks: facts or fashion? (reply to A. D. Edgar's discussion paper). Contrib Mineral Petrol 73: 432-434

Edwards C, Menzies M, Thirlwall M (1991) Evidence from Muriah, Indonesia, for the interplay of supra-subduction zone and intraplate processes in the genesis of potassic alkaline magmas. J Petrol 32: 555-592

Goodenough KM, Wall F, Merriman D (2018) The Rare Earth Elements: Demand, global resources, and challenges for resourcing future generations. Nat Resour Res 27: 201-216

Hamilton W (1977) Subduction in the Indonesian region. A. Geophys Union Maurice Ewing Series 1: 15-31

Hoshino M, Sanematsu K, Watanabe Y (2016) REE Mineralogy and Resources, Handbook on the Physics and Chemistry of Rare Earths: 129-291. Elsevier

Hutchison CS (1981) Review of the Indonesian volcanic arc. The geology and tectonics of eastern Indonesia. Spec Publ Geol Res Dev Centre 2: 65-80

Hutchison CS (1982) Indonesia. In: Andesites: orogenic andesites and related rocks: 207-224. Wiley, New York

Le Couteur P (2011) Geological report on the Chambe Basin area of exclusive prospecting license EPL0325/11 Mulanje Massif, Southern Malawi, East Africa. 1-101, Vancoucer, Micron Geological Ltd

Leterrier J, Yuwono YS, Soeria-Atmadja R, Maury RC (1990) Potassic volcanism in Central Java and South Sulawesi, Indonesia. J Southeast Asian Earth Sci 4: 171-187

Li Z, Hu JZ (2017) World rare earth resources survey and development utilization trend. Mod Min 33: 97-105 (In Chinese with English abstract).

Li YHM, Zhao WW, Zhou MF (2017) Nature of parent rocks, mineralization styles and ore genesis of regolith hosted REE deposits in South China: An integrated genetic model. J Asian Earth Sci 148: 65-95

Mcbirney AR, Serva L, Guerra M, Connor CB (2003) Volcanic and seismic hazards at a proposed nuclear power site in Central Java. J Volcanol Geotherm Res 126: 11-30

Mukai H, Kon Y, Sanematsu K, Takahashi Y, Ito M (2020) Microscopic analyses of weathered granite in ion-adsorption rare earth deposit of Jianxi Province, China. Sci Rep 10: 20194

Qin F, Tan J, Zhou YQ, Meng XL (2019) Characteristics and genesis of ion-adsorbed rare-earth deposits in volcanic weathering crust in Chongzuo area of Guangxi. Mineral Res Geol 033: 234-241 (in Chinese with English abstract)

Rocha A, Schissel D, Sprecher A, De Tarso P, Goode J (2013) Process development for the Serra Verde weathered crust elution-deposited rare earth deposit in Brazil. Proceedings of the 52nd Conference of Metallurgists (COM 2013)

Sanematsu K, Watanabe Y (2016) Characteristics and genesis of ion adsorption-type rare earth element deposits. Rev Econ Geol. Soc Econ Geol: 55-79

Sanematsu K, Murakami H, Watanabe Y, Duangsurigna S, Siphandone V (2009) Enrichment of rare earth elements (REE) in granitic rocks and their weathered crusts in central and southern Laos. Bull Geol Surv Japan 60: 527-558

Setiawan I, Takahashi R, Imai A (2017) Petrochemistry of granitoids in Sibolga and its surrounding areas, North Sumatra, Indonesia. Resour Geol 67(3): 254-278

Wang ZY, Fan HR, Zhou L, Yang KF, She HD (2020) Carbonatite-related REE deposits: An overview. Minerals 10: 965

Wu CY, Huang DH, Guo ZX (1990) REE geochemistry in the weathered crust of granites, Longnan area, Jiangxi Province. Acta Geol Sin Engl 3: 193-209

Xie YL, Hou, ZQ, Goldfarb RJ, Guo X, Wang L (2016) Rare Earth Element Deposits in China. Rev Econ Geol. Soc Econ Geol: 115-136

Zhang SJ, Zhang, LW, Zhang YW, Shang L, Li JB (2020) Summarize on rare earth mineral resources and their distribution at home and abroad. Inorg Chem Ind 52: 9-16 (In Chinese with English abstract)